Geophysical Research Letters

RESEARCH LETTER
10.1029/2021GL095341

Key Points:

- An impact crater database surrounding the Chang'e-5 site was produced
- Crater ages are constrained either by CSFD or crater morphology or degradation methods
- Ejecta are mainly from local craters, delivered by Copernican-aged (>200 Ma) craters

Supporting Information:

Supporting Information may be found in the online version of this article.

Correspondence to:

L. Xiao and J. W. Head,
longxiao@cug.edu.cn;
James_Head@brown.edu

Citation:

Qian, Y., Xiao, L., Head, J. W., Wöhler, C., Bugiolacchi, R., Wilhelm, T., et al. (2021). Copernican-aged (<200 Ma) impact ejecta at the Chang'e-5 landing site: Statistical evidence from crater morphology, morphometry, and degradation models. *Geophysical Research Letters*, *48*, e2021GL095341. https://doi.org/10.1029/2021GL095341

Received 23 JUL 2021
Accepted 24 SEP 2021

Copernican-Aged (<200 Ma) Impact Ejecta at the Chang'e-5 Landing Site: Statistical Evidence From Crater Morphology, Morphometry, and Degradation Models

Yuqi Qian[1,2], Long Xiao[1,3], James W. Head[2], Christian Wöhler[4], Roberto Bugiolacchi[5], Thorsten Wilhelm[4], Stephanie Althoff[4], Binlong Ye[6], Qi He[1], Yuefeng Yuan[7], and Siyuan Zhao[1]

[1]State Key Laboratory of Geological Processes and Mineral Resources, School of Earth Sciences, China University of Geosciences, Planetary Science Institute, Wuhan, China, [2]Department of Earth, Environmental, and Planetary Sciences, Brown University, Providence, RI, USA, [3]Center for Excellence in Comparative Planetology, Chinese Academy of Sciences, Hefei, China, [4]Image Analysis Group, TU Dortmund University, Dortmund, Germany, [5]State Key Laboratory of Lunar and Planetary Sciences, Macau University of Science and Technology, Macau, China, [6]Department of Earth Sciences and Laboratory for Space Research, University of Hong Kong, Hong Kong, China, [7]China University of Geosciences, Institute of Geophysics and Geomatics, Wuhan, China

Abstract Chang'e-5 successfully returned ~1,731 g of lunar samples on December 17, 2020. We systematically studied the morphology and morphometry of craters surrounding the Chang'e-5 site based on high-resolution images. A key ejecta source crater database was produced, incorporating their morphometrical parameters, excavation depth, target rock types, and ages from either crater counting, crater morphology or degradation methods. We found that (a) the regolith at the Chang'e-5 site is ~4–6 m thick, (b) ejecta are primarily from five proximal craters, including Xu Guangqi, dominantly with ages <200 Ma; (c) distal materials are mainly from Harpalus, Copernicus, Aristarchus, and Mairan G craters; (d) the drill samples are likely to be mainly from Impact Crater (IC)-261 and IC-265 particles at the top and the contribution of Xu Guangqi increases with depth; (e) the ejecta of Xu Guangqi would buried preexisting materials but probably overturned by postimpacts.

Plain Language Summary The Chang'e-5 mission, China's first lunar sample-return mission, successfully landed on the Moon on December 1, 2020, at 43.06°N, 51.92°W, and returned 1,731 g of lunar soil samples. Because of the potentially large contribution from local impact craters to the collected samples, we conducted this research to study these craters based on high-resolution orbital data. Our results support the hypothesis that local craters are the major ejecta sources, mainly from Impact Crater (IC)-259, IC-261, IC-265, IC-266, and Xu Guangqi crater. Of these, Xu Guangqi is the most critical ejecta source crater and Chang'e-5 landed on its ejecta deposit. Its ejecta would bury preexisting materials, such as those from distant craters Harpalus, Copernicus, Aristarchus, and Mairan G, but subsequent craters may redistribute buried materials again, and represented in the regolith sampled by Chang'e-5.

1. Introduction

Chang'e-5 (CE-5) is China's first lunar sample-return mission. It landed in northern Oceanus Procellarum on December 1, 2020, at 43.06°N, 51.92°W (Wang et al., 2021). 1,731 g of lunar regolith was collected and are currently under laboratory investigations.

The CE-5 site (Statio Tianchuan, IAU-name) is located within Eratosthenian-aged intermediate-Ti mare basalts (labeled as Em4/P58 by Qian, Xiao, Wang, et al., 2021), with an average thickness of ~51 m, a total volume between 1,450 and 2,350 km^3 (Qian, Xiao, Head, van der Bogert, et al., 2021), and a ~7 m thick regolith superposed (Yue et al., 2019). The CE-5 sample-return strategy included a 2 m-drill (~1 m was re-covered) and a surface sampling device (Deng et al., 2021). The returned samples are thus likely to contain materials from different sources, including local basalts mixed by vertical and lateral transportation with exotic materials (Huang et al., 2017; Liu, Michael, Zuschneid, et al., 2021). The local mare materials might be erupted from Rima Sharp (Qian, Xiao, Head, & Wilson et al., 2021) and will help to better understand the nature of late-stage volcanism, deep mantle properties, and lunar chronologies; the distal materials would

help to reveal subsurface composition at a distance from the impacting site, and also calibrate chronology functions (van der Bogert & Hiesinger, 2020). Therefore, a thorough understanding of the provenance of the CE-5 samples could help the sample analysts locate the key scientific questions and maximize the outcome of CE-5 from a previously unsampled young area (J. Liu et al., 2020).

Different researchers have studied the possible distal ejecta sources for the CE-5 region. Xie et al. (2020) proposed that Aristarchus (~8%), Copernicus (~2%), Sharp B (~1%), and Harding (~0.4%) craters contributed the most distal ejecta to Em4/P58 according to the ballistic sedimentation model. Qian, Xiao, Wang, et al. (2021) directly tracked the ejecta rays surrounding the CE-5 site based on albedos and compositions, and estimated their percentages using a power law model. They concluded that the admixed impact ejecta are mainly from Harpalus (~6%), Copernicus (~2%), and Aristarchus (~1%) craters. By also tracing the secondaries close to the landing site, Qiao et al. (2021) supported the interpretation that distal materials are from Copernicus and Harpalus craters for the SE-NW and NE-SW ejecta. In addition, Fu et al. (2021) studied the nonmare materials by unmixing 12 FeO-Th endmembers in the northern Oceanus Procellarum, concluding that Aristarchus crater contributed highly evolved materials, and thorium is indigenous to basalts. T. Liu et al. (2020) proposed a spatially resolved numerical model to calculate the basin-derived melt abundance from cumulative lateral and vertical mixing. Using this model, Liu, Michael, Zhu, and Wünnemann et al. (2021) suggested that there is ~40% nonmare materials at the CE-5 site, mainly from the Imbrium basin; and distal materials are from Sharp B, Harding, Copernicus, and Aristarchus craters.

In summary, most previous studies focus on the broad CE-5 region in northern Oceanus Procellarum, and a detailed investigation of the local craters surrounding the CE-5 site has not been reported. However, lunar regolith is mainly from comminution by local impacts and controlled by bedrock composition based on the Apollo/Luna results (Hörz et al., 1991; McKay et al., 1991): >95% of the regolith is locally derived (<5 km), only <1% comes from sources >10 km distant. Because of the significance of studying impact melts/breccias by modern techniques such as Ar-Ar and U-Pb chronologies and geochemical tracing (Joy et al., 2010; Mercer et al., 2015), it is critical to constrain the local ejecta contributors in the vicinity of the CE-5 site.

Benefitting from the acquisition of high-resolution Lunar Reconnaissance Orbiter Camera (LROC) images (Robinson et al., 2010), it is now possible to analyze the impact craters surrounding the CE-5 site, and estimate the ejecta delivered by them. Here we show that the morphology and morphometry of small craters (<1 km) and crater size-frequency distribution (CSFD) measurements on the continuous ejecta of large craters (>1 km) could constrain their formation ages, which can be compared with the laboratory dating of impact melts/breccias. In addition, even smaller craters (<250 m) can be used to obtain lunar regolith thickness based on the concentric crater method. All results will help the CE-5 sample analysis and data interpretations.

2. Data and Methods

2.1. Data

The morphology of all craters were studied based on LROC NAC data (1–1.5 m/pixel; Robinson et al., 2010) after registration using ISIS3 (Sides et al., 2017). To measure the morphometry of small craters (<1 km), a shape from shading-based method was used to produce NAC DEMs (Zhang et al., 2020); and three NAC DEMs were constructed (M1348581418L, M1173414625L/R). All NAC images used are listed in Table S1 in Supporting Information S1. In addition, SLDEM2015 (Barker et al., 2016) is used to measure the morphometry of large craters, Kaguya TC Morning Map (Haruyama et al., 2008) and LROC Wide Angle Camera (LRO WAC; Robinson et al., 2010) data are used as basemaps.

2.2. Regolith Thickness

We updated the regolith thickness maps of the CE-5 landing region (41°–45°N, 49°–69°W) produced by Yue et al. (2019, their Figure 3), benefiting from the accurate landing site coordinates determination since then. A new regolith thickness map (Figure 1c, 42°–44°N, 50°–53°W) was created based on the small fresh crater (<250 m) morphologies. This method relies on the transition of simple, flat-bottomed/central mound, and concentric craters (Figure S1 in Supporting Information S1) with increasing regolith thickness (Oberbeck

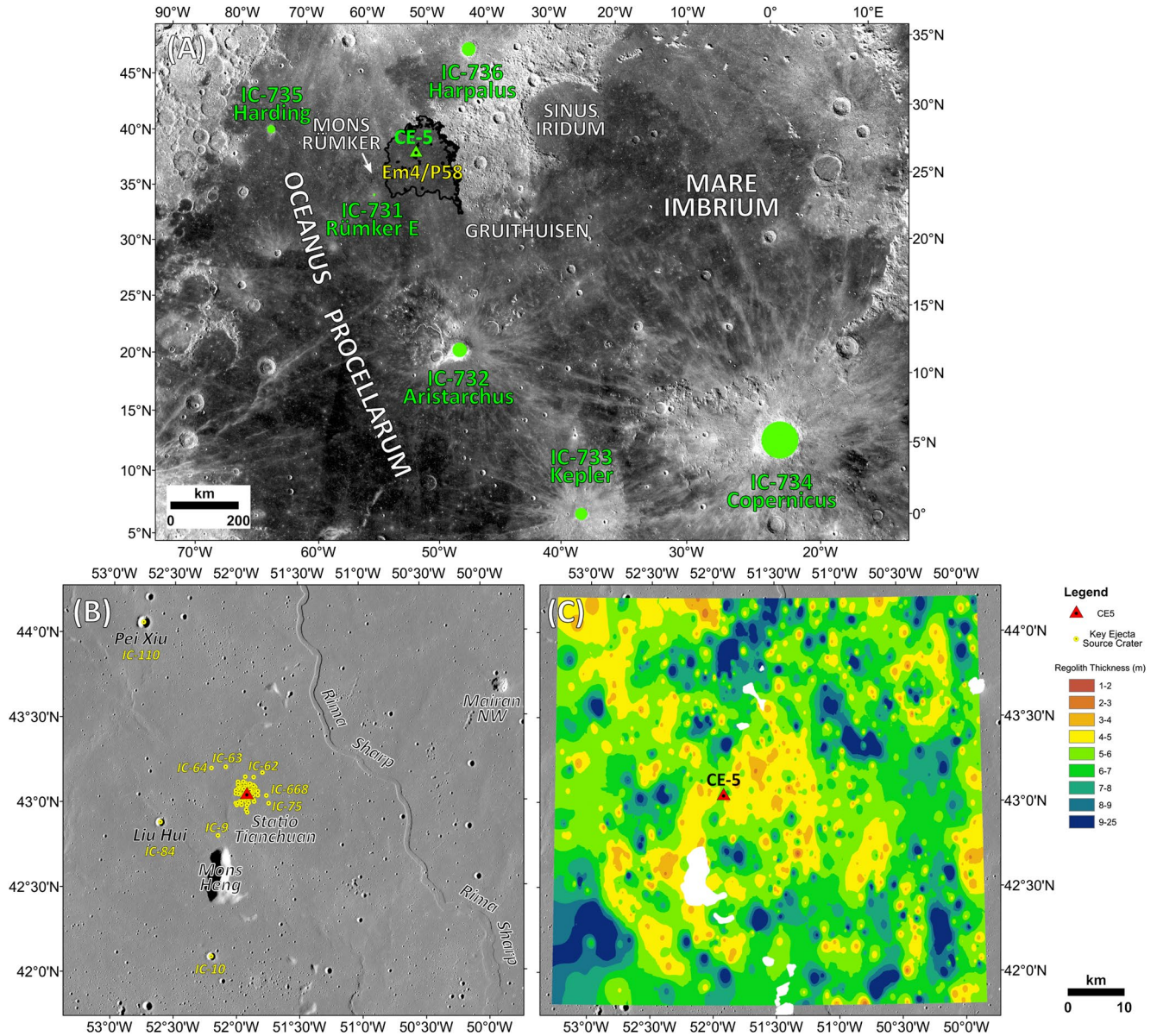

Figure 1. (a) Context of CE-5 site in Norther Oceanus Procellarum. Green dots represent key distal impact craters. The black line represents the geological boundary of Em4/P58 (Qian, Xiao, Head, van der Bogert, et al., 2021). The basemap is a LROC WAC image (Robinson et al., 2010). (b) CE-5 landing region. Yellow dots represent key ejecta source craters. The basemap is a Kaguya TC Morning Map image (Haruyama et al., 2008). (c) Regolith thickness of the landing site (Section 3.1). Craters used to calculate regolith thickness are shown in Figure S2 and Table S5 in Supporting Information S1.

& Quaide, 1968). In practice, only concentric craters were used (Yue et al., 2019), and the diameter from rim-to-rim (DA) and of the inner ring (DF) were measured on the NAC images to obtain regolith thickness, using their Equation 1.

2.3. Ejecta Thickness and Key Ejecta Source Selection

To select potential craters whose ejecta contribution are nonnegligible, we first applied the power law model of ejecta thickness modified by Huang et al. (2018). The model assumes the relation between r (the distance to the crater center), R (crater radius), and T (ejecta thickness) is: $T = 3.95\ R^{0.399}(r/R)^{-3}$. The excavation efficiency (μ) of ejecta is $\mu = 2.25 \times 10^{-5}\ r^{0.87}$ adopting half of excavation efficiency of Oberbeck (1975)

according to Petro and Pieters (2006), and the total ejecta thickness equals the sum of distal ejecta and excavated local material.

All key ejecta source craters were selected by the criteria described in Text S1; Tables S2 and S3 in Supporting Information S1, excluding Imbrian-aged ones. In this way, 736 craters were selected (labeled from IC-1 to 736, IC = Impact Crater), and 209 craters with >0.1 cm ejecta were further studied as a database (Table S4 in Supporting Information S1) to constrain their morphology types, target properties, excavation depth, and formation ages. Their topographic profiles were acquired from the NAC DEMs and classified into good/medium/bad qualities; medium/bad ones in most cases are near the resolution limit or disturbed by other craters. Then their morphometric parameters (i.e., diameter, diameter calibrated, depth, depth/diameter, and maximum slope) were measured based on profiles.

2.4. Target Rock and Excavation Depth

To constrain the properties of the materials transported to the site, the target type of each critical crater was determined and classified into "mare" or "highland," and further into geological units according to the boundaries of Hiesinger et al. (2011) and Qian, Xiao, Head, van der Bogert, et al. (2021). The excavation depth of each crater was calculated by the depth of transient crater (Melosh, 1989). For those craters within Em4/P58, it was determined whether or not each crater excavated the underlying low-Ti mare basalts based on Kaguya MI TiO_2 abundance data (Lemelin et al., 2016).

2.5. Impact Crater Formation Age

The formation age of small craters (<1 km) was computed by crater morphology and degradation method separately. For the first method, we classified each crater into Basilevsky (1976) classes (A/AB/B/BC/C) on the basis of the morphometry measurements and NAC-based morphologies. Using the relationship of each class crater and their residence time on the lunar surface (Figure 4 in Basilevsky, 1976), the lower/upper limit age of each crater was determined (Table S4 in Supporting Information S1).

The crater degradation model is developed quantitatively from the acquisition of lunar high-resolution topography (Fassett & Thomson, 2014; Xie et al., 2017). Here we used nine different crater degradation models (Models 1/2/2'/3/3'/4/4'/5/5') to estimate crater ages if having good profile quality (51 in total), based on the crater degradation models by Fassett and Thomson (2014) and Xie et al. (2017), and a locally calibrated crater diffusion rate for Models 4/4'/5/5'. The local diffusion rate was derived from comparing the CSFD of 10–100 m-diameter craters measured by an automatic crater detector (Wilhelm & Wöhler, 2021) and a Monte Carlo cratering simulation (Bugiolacchi & Wöhler, 2020) after degradation. Details of, and comparisons between the different degradation methods are given in Text S2 and S3 in Supporting Information S1, and an example is given in Figure S4 in Supporting Information S1. We find Model 1 (a quantitative model based on Xie et al., 2017), and Model 4 (a simplified model based on the depth/diameter ratio with a locally calibrated diffusion rate) can give the best crater age estimations (Text S3 in Supporting Information S1). Therefore, the following discussions of crater ages are mainly based on the results of Models 1 and 4.

For large craters (>1 km; Aristarchus, Kepler, Copernicus, Harding) which have been well studied, their ages were taken from the literature (Table 1); for 10 additional large craters (IC-10/12/17/19/22/84/110/115/731/736), their absolute model ages (AMAs) were obtained by CSFD measurements on NAC images, applying CraterTools (Kneissl et al., 2011) and Craterstats (Michael & Neukum, 2010), and the production and chronology function of Neukum et al. (2001). Crater counting areas are on the continuous ejecta (Figure S10 in Supporting Information S1), except for IC-736, on impact melt ponds (Figure S12 in Supporting Information S1). Uncertainties of the CSFD method are discussed in Text S4 in Supporting Information S1, especially involving <50 m craters, whose population may reach equilibrium after a few tens of Ma (Bugiolacchi & Wöhler, 2020).

Table 1
Twenty-Nine Most Critical Ejecta Source Craters

Impact crater ID	Longitude (°)	Latitude (°)	Diameter (m)	Ejecta thickness (cm)	Target geologic unit	Excavation depth (m)	Absolute age	Morphology age (class)[f]	Degradation age[f]
Small Crater (<1 km)									
IC-396 (Xu Guangqi)	−51.932	43.066	419	404.6	Em4/P58	35.2	/	74–492 Ma (B)	60 Ma | 218 Ma
IC-265	−51.920	43.059	98	312.7	Em4/P58	8.2	/	124–248 Ma (C)	140 Ma | 57 Ma
IC-266	−51.917	43.054	72	45.6	Em4/P58	6.1	/	91–182 Ma (C)	/
IC-259	−51.916	43.059	11	33.9	Em4/P58	1.0	/	6–15 Ma (BC)	/
IC-261	−51.915	43.058	9	23.5	Em4/P58	0.7	/	5–12 Ma (BC)	/
IC-320	−51.909	43.064	104	19.6	Em4/P58	8.7	/	52–131 Ma (BC)	120 Ma | 57 Ma
IC-406	−51.906	43.072	187	17.0	Em4/P58	15.7	/	121–302 Ma (BC)	120 Ma | 110 Ma
IC-400	−51.915	43.049	111	16.3	Em4/P58	9.3		56–140 Ma (BC)	/
IC-268	−51.914	43.059	25	15.9	Em4/P58	2.1	/	32–65 Ma (C)	/
IC-263	−51.917	43.059	20	14.1	Em4/P58	1.7	/	26–52 Ma (C)	/
IC-440	−51.908	43.049	121	12.1	Em4/P58	10.1	/	152–305 Ma (C)	/
IC-262	−51.917	43.058	10	10.9	Em4/P58	0.8	/	6–14 Ma (BC)	/
IC-306	−51.917	43.058	12	8.6	Em4/P58	1.0	/	16–32 Ma (C)	/
IC-553	−51.911	43.104	368	7.1	Em4/P58	30.9	/	62–410 Ma (B)	140 Ma | 244 Ma
IC-322	−51.907	43.059	60	5.7	Em4/P58	5.1	/	76–152 Ma (C)	/
Large Crater (> 1 km)									
IC-736 (Harpalus)	−43.490	52.730	39,770	10.2	Undefined Mare	3340.7	490 ± 60 Ma	/	/
IC-734 (Copernicus)	−20.060	9.640	94,300	7.6	Undefined Mare	7921.2	796 Ma[a]	/	/
IC-732 (Aristarchus)	−47.490	23.740	40,140	2.7	Undefined Mare	3371.8	280 Ma[b]		
IC-17 (Mairan G)	−50.828	40.902	5,892	1.0	Em4/P58	494.9, Penetrating[e]	480 ± 50 Ma		
IC-84 (Liu Hui)	−52.611	42.886	1,675	0.9	Em4/P58	140.7	57 ± 5 Ma[h]		
IC-735 (Harding)	−71.680	43.540	23,040	0.9	Undefined Mare	1935.4	881 Ma[c]		
IC-19 (Louville D)	−52.144	46.853	7,021	0.5	P10 (3.4 Ga)	589.8	98 ± 9 Ma		
IC-110 (Pei Xiu)	−52.758	44.062	2,211	0.2	Em4/P58	185.8, Penetrating[e]	52 ± 4 Ma		
IC-733 (Kepler)	−38.000	8.110	30,120	0.2	Undefined Mare	2530.1	625–950 Ma[d]		
IC-22 (Rümker H)	−52.754	40.334	4,038	0.2	Em4/P58	339.2, Penetrating[e]	67 ± 4 Ma		
IC-10	−52.200	42.097	1,605	0.1	Em4/P58	134.8, Penetrating[e]	96 ± 8 Ma		
IC-731 (Rümker E)	−57.140	38.640	6,760	0.1	P9 (3.5 Ga)	567.8	27 ± 6 Ma		
IC-12	−52.684	41.713	2,144	0.1	Em4/P58	180.1, Penetrating[e]	170 ± 20 Ma		
IC-115 (Louville K)	−55.220	46.783	5,135	0.1	P10 (3.4 Ga)	431.3	39 ± 3 Ma[h]		

Note. The full table is appended in Table S4 in Supporting Information S1.

[a]Iqbal et al. (2020). [b]Zanetti et al. (2017). [c]Xie et al. (2020). [d]Koenig et al. (1977). [e]"Penetrating" means this crater is within Em4/P58 and can penetrate through Em4/P58 to excavate the underlaying Imbrian-aged mare basalts. [f]Based on the crater morphology method of Basilevsky (1976) (Section 2.5). [g]Based on the crater degradation Model 1 and Model 4, respectively (Section 2.5; Text S2 and S3 in Supporting Information S1). [h]CSFD ages may influenced by involving craters <50 m.

3. Results

3.1. Regolith Thickness

The regolith thickness (Figure 1c) within 42°–44°N, 50°–53°W was obtained through the concentric crater method (Section 2.2). In total, the DA and DF of 1,084 craters were measured (Figure S2a and Table S5 in Supporting Information S1). This region has a mean regolith thickness of ~6.1 m; ~31% and ~88% of the area has a thickness between 5–6 and 4–8 m (Figure S2b in Supporting Information S1), respectively. The vicinity of CE-5 site has a thickness between 4 and 6 m. The mean regolith thickness is slightly smaller than Yue et al.'s (2019) results (~7.2 ± 2.6 m). Compared with Yue et al. (2019), the results here have a much higher resolution that may help penetration radar interpretations (Shen et al., 2021).

3.2. Ejecta Contribution

The ejecta thickness of each crater was calculated using a power law model (Section 2.3). In total, these 209 craters contributed ~1,096 cm of ejecta to the landing site. Only 48 craters are able to provide >1 cm ejecta, comprising ~95% of all ejecta; ejecta contributions from other craters are nearly negligible. Results of 29 critical ejecta source craters (>5 cm ejecta or >1 km in diameter) are shown in Figure 2 and Table 1. The top five craters, Xu Guangqi (~405 cm), IC-265 (~313 cm), IC-266 (~46 cm), IC-259 (~34 cm), and IC-261 (~24 cm) transported >20 cm ejecta to the site, however contributing ~75% of all ejecta. More than half of the ejecta is from Xu Guangqi (~37%) and IC-265 (~29%), which are 424 and 89 m away from the site.

Key sources outside Em4/P58 include Harpalus, Copernicus, Aristarchus, Harding, Louville D, Kepler, Rümker E, and Louville K (Figure 1a), overall contributing ~2% ejecta to the site; ejecta are thus dominated by local Em4/P58 materials. Therefore, the isotopic ages of CE-5 samples will be controlled by the local basalts.

3.3. Impact Crater Age

The small crater (<1 km) ages were estimated by the crater morphology or degradation method (Section 2.5). As shown by Figures 3a–3d and Figure S17 in Supporting Information S1, also because the CE-5 site is on an Eratosthenian-aged basalts (Qian, Xiao, Head, van der Bogert, et al., 2021), all studied craters are Copernican or Late-Eratosthenian-aged; ~75% of the craters are inferred to be younger than 150 Ma. The three youngest craters are IC-258 (1–7 Ma), IC-260 (1–8 Ma), and IC-575 (0–11 Ma), with diameters of 13, 15, and 145 m (Figures S19a–S19c in Supporting Information S1), respectively. IC-575 is a fresh, concentric crater; the abundant boulders on its rim, wall, and floor suggests it has an extremely young age (Hörz et al., 2020) (Figure S19c in Supporting Information S1). IC-75 (694–1388 Ma, 285 m-diameter) is the oldest crater of those measured, belonging to morphology class C (Figure S19d in Supporting Information S1).

Besides, the automatic crater detection coupled with the crater degradation Model 4 (Text S3 in Supporting Information S1) show that crater numbers increase toward young ages and reach the highest number in the 0–10 Ma bin (Figure 3d). Although the automatic method may suffer from misidentifications, the trend is clear and is also seen in the manual-determined database (Figures 3a and 3c). These craters cannot provide considerable ejecta and are therefore excluded from the database.

Ten large craters (>1 km) were dated by the CSFD method (Figure S11 in Supporting Information S1; uncertainties are discussed in Text S4 in Supporting Information S1), and the ages of Aristarchus (280 Ma; Zanetti et al., 2017), Kepler (625–950 Ma; Koenig et al., 1977), Copernicus (796 Ma; Iqbal et al., 2020), and Harding (881 Ma, Xie et al., 2017) were taken from the literature (Table 1). Seven craters dated are younger than 100 Ma, including Rümker E (27 ± 6 Ma), Louville K (39 ± 3 Ma), Pei Xiu (52 ± 4 Ma), Liu Hui (57 ± 5 Ma), Rümker H (67 ± 4 Ma), IC-10 (96 ± 8 Ma), and Louville D (98 ± 9 Ma). Rümker E is the youngest large crater, with rays reaching >70 km (Figure 2a), indicating an extremely young age.

The age of Harpalus is more controversial, but even critical because the prominent NE-SW rays overlying Em4/P58 are either from Sharp B or Harpalus or both. Qian, Xiao, Wang, et al. (2021) proposed that Sharp B is not the source but Harpalus instead, because directly dating Sharp B and Harpalus on their ejecta would

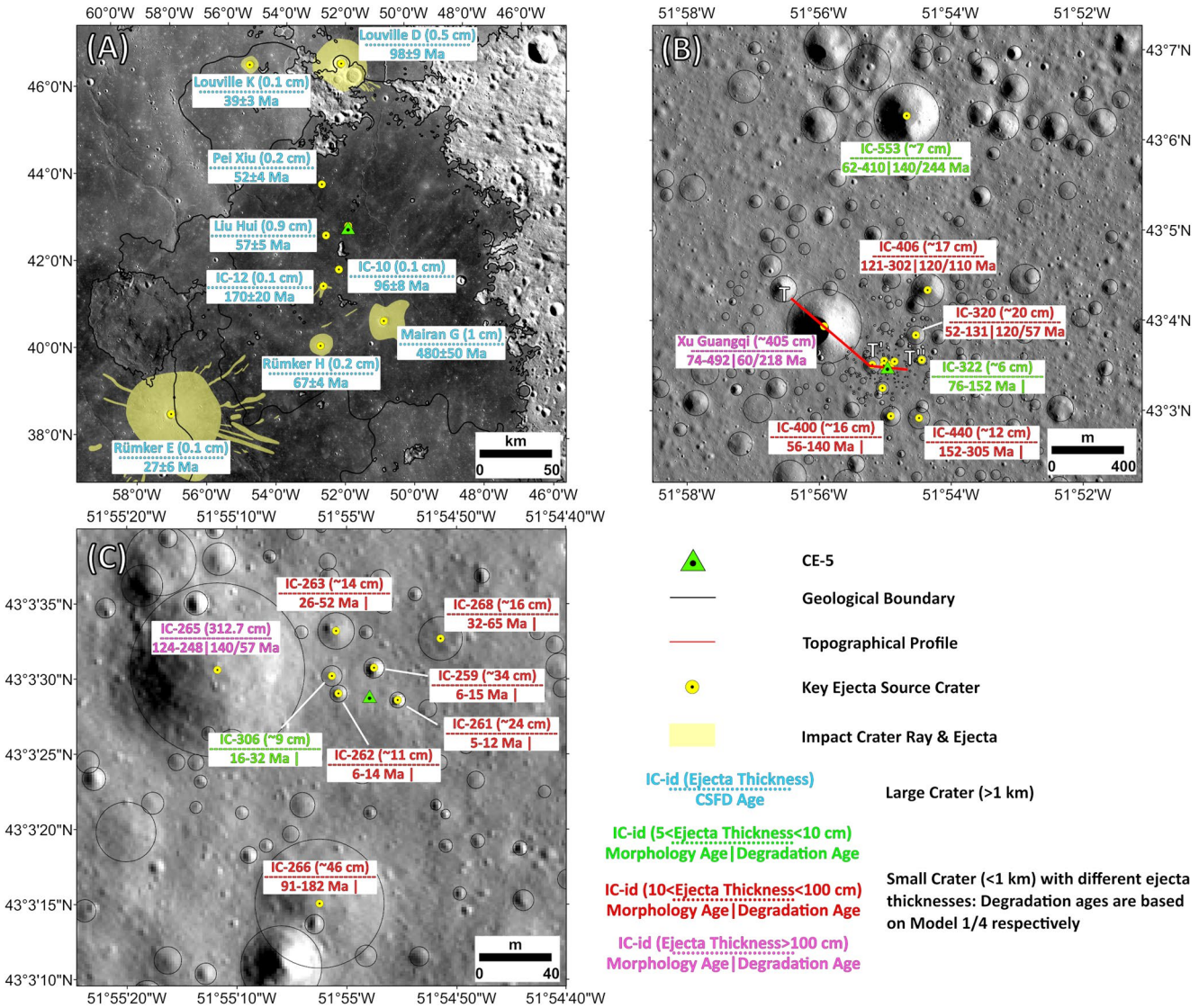

Figure 2. Ejecta contribution and corresponding ages of the 15 most important small craters (<1 km) and 14 large craters (>1 km, blue text) (Table 1). The ages of small craters are estimated by either the crater morphology method (before "|") or crater degradation Model 1/4 (Section 2.5; after "|") or both. Crater labeled in green, red, and purple contributed 5–10 cm, 10–100 cm, and >100 cm of ejecta to the CE-5 site, respectively. (a) Ejecta source craters in northern Oceanus Procellarum. The basemap is a LROC WAC image. (b and c) Ejecta source craters around the CE-5 site. (c) A zoom-in view of (b). The basemap is a LROC NAC image.

yield unreliable ages due to self-secondaries and the rough surface. Alternatively, using high-resolution NAC images, we found two impact melt ponds within the west and east wall of Harpalus (Figures S12a–S12c in Supporting Information S1). CSFD measurements on these two flat ponds formed concurrently with the crater should provide more reliable ages than the rough ejecta deposit. On this basis, the age of Harpalus was concluded to be ~490 Ma (Figures S12d and S12e in Supporting Information S1), younger than the CE-5 basalts and probably transporting distal materials to the site.

4. Discussion

4.1. Ejecta Composition

The potential ejecta compositions transported to the CE-5 site are constrained by the excavated material amounts and the target rock properties. According to the investigations of key craters (Table S4 in Sup-

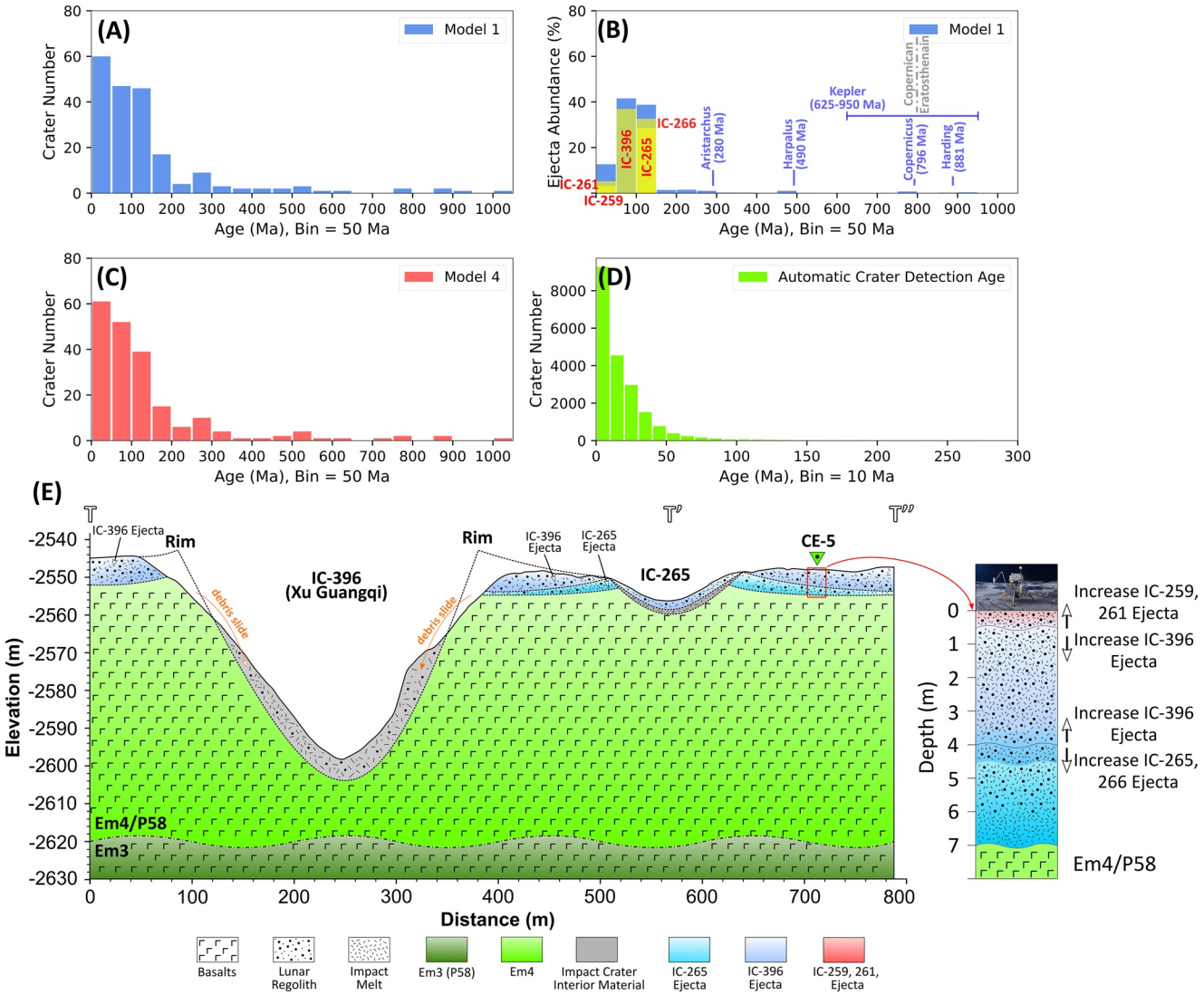

Figure 3. (a) Model 1 results of crater ages. (b) Model 1 results of crater ages and corresponding ejecta abundance. (c) Model 4 results of crater ages. (d) Automatic crater detection ages derived from local calibrated diffusion rates (Text S2 in Supporting Information S1); (e) Stratigraphy of the CE-5 landing site. The ages of IC-265 and Xu Guangqi crater are discussed in Section 4.3. Model 1 and Model 4 estimate ages of 209 craters. Automatic crater detection technique estimates ages of 37,765 craters. The ground track of T-T′-T″ can be found in Figure 2b.

porting Information S1), only Harpalus, Copernicus, Aristarchus, Harding, Louville D, Kepler, Rümker E, and Louville K are outside Em4/P58, and highly likely to deliver distal materials; they occupy ~2% of all expected ejecta. Another type of crater that may contribute different materials are those within Em4/P58 but penetrating through the ~39–63 m thick intermediate-Ti basalts (Qian, Xiao, Head, van der Bogert, et al., 2021) and excavating the underlying Imbrian-aged low-Ti basalts. This type of crater includes Mairan G, Pei Xiu, Rümker H, IC-10, and IC-12 (Figure S20 in Supporting Information S1), able to excavate 495, 186, 339, 135, and 180 m deep materials, respectively. However, the total amount of ejecta derived by the local-penetrating craters is minor (~0.1% of all ejecta), compared with distal large craters, agreeing with the results from spatially resolved numerical model (Liu, Michael, Zhu, & Wünnemann, et al., 2021).

All the other craters (190 in number, Table S4 in Supporting Information S1) within Em4/P58, but not penetrating through the overlaying unit, still impact and transport the same type of local material as seen at the CE-5 site. If we only consider distal/different materials (ejecta thickness = distal crater ejecta + excavated local material, Section 2.3), the total distal/different ejecta thickness is ~8 cm, and if totally mixed with the top ~74 cm regolith by gardening (Costello et al., 2020; Qian, Xiao, Wang, et al., 2021), which leads us to

conclude that the distal/different materials are likely to be mainly from Harpalus (~6%), Copernicus (~2%), Aristarchus (~1%), and Mairan G (~1%) craters.

4.2. Ejecta Age

We have compared crater ages determined by different methods (Text S3 in Supporting Information S1) and find that they generally follow the same trend: the older the degradation age, the older the morphology age, and vice versa. The relation between the results of Model 1 and other models are shown in Figure S8 in Supporting Information S1. All models have a good correlation with each other, in terms of r values (≥0.8). There may be some systematic difference from model assumptions that can be tested by samples.

In terms of ejecta volume from different-aged craters, all source craters are Copernican (<800 Ma) or Late-Eratosthenian-aged (800–1,050 Ma) (Figure 3b); ~93% of the ejecta have a source crater younger than 150 Ma, mainly from IC-261 (~2%), IC-259 (~3%), IC-266 (~4%), IC-265 (~29%), and Xu Guangqi (~37%), especially IC-265 and Xu Guangqi. These five craters alone contributed ~75% of the ejecta to the site; therefore, we predict that impact melt sampled by CE-5 are dominated by young ages (<200 Ma), mainly representing ejecta derived from IC-265 and Xu Guangqi.

4.3. Stratigraphy of the CE-5 Site and Ages of IC-259, 261, 265, 266, and Xu Guangqi

A stratigraphic column was constructed of the CE-5 site (Figure 3e) in order to better understand the sample provenance and subsurface structures. The CE-5 site is located on a basaltic regolith developing from solidified lava flow protolith (Head & Wilson, 2020). The impact ejecta at the CE-5 site are expected to be mainly from Xu Guangqi, IC-265, IC-266, IC-259, and IC-261, contributing ~75% of all the ejecta (Table 1). IC-265 (124–248 Ma) and IC-266 (91–182 Ma) are two class C craters with subdued morphology and no exposed boulders (Figure 2c), indicating relatively older ages than the other three. Therefore, their ejecta are expected more at the bottom of the column (Figure 3e), overlying the Eratosthenian-aged intermediate-Ti bedrock (Qian, Xiao, Head, van der Bogert, et al., 2021).

Above the IC-265 and IC-266 ejecta are the Xu Guangqi (IC-396) ejecta. In terms of expected ejecta volume, Xu Guangqi is the most significant crater among all studied craters because it is the largest (419 m-diameter) crater adjacent to the site (424 m-distance). Qiao et al. (2021) studied this crater and proposed that it is older than Copernicus crater because Copernicus secondaries appear to be superposed on Xu Guangqi ejecta blanket. However, the small secondary craters (a few tens of meters) described by Qiao et al. (2021d) are unlikely to be from Copernicus (~796 Ma; Iqbal et al., 2020), because craters in this size are unlikely to be preserved for >200 Ma on the lunar surface (Basilevsky, 1976; Fassett & Thomson, 2014). In addition, abundant boulders occur on the rim, wall, and floor of Xu Guangqi, especially on the southeast wall (Figure 2b and Figure S19e in Supporting Information S1). The survival time of meter-sized boulders on the lunar surface is about 150–300 Ma (Basilevsky et al., 2013), suggesting that Xu Guangqi is younger than 150–300 Ma. Furthermore, according to crater degradation Model 1 (Section 2.4), the age of Xu Guangqi is interpreted to be ~60 Ma, at the lower end of the crater morphology age (74–492 Ma). Therefore, Xu Guangqi may have formed ~60–75 Ma ago; its ejecta overlying the IC-265 and IC-266 ejecta (Figure 3e). The age of Xu Guangqi derived from Model 1 and Model 4 is further compared in Figure S15 in Supporting Information S1. It is also possible that Xu Guangqi has an age of ~200 Ma based on Model 4, but that would not change the main conclusions.

Xu Guangqi penetrated through a depth of ~35 m, not deep enough to excavate the underlying low-Ti basalts, but certainly deliver deep basalts, possibly affecting their isotopic systems and generating impact melts. All these materials, if sampled, can be used to date the age of Xu Guangqi. The retrieved samples can test and improve crater degradation models on a flat mare surface without complex geology such as Apollo sites (Cone, North and South Ray craters, Figure S16 in Supporting Information S1). In addition, Robinson (2021) used a newly obtained LROC NAC DTM to study samples that might have been collect by CE-5, concluding that the crater we designate IC-265 formed on the ejecta deposit of the larger crater Xu Guangqi, and that both of these craters sampled the Em4/P58 unit. These findings are consistent with our results.

At the top of the geological column (Figure 3e) are the ejecta from IC-259 and IC-261. They are small (11 and 9 m diameter) craters next to the CE-5 site (16 and 14 m distance). IC-259 (6–15 Ma) and IC-261 (5–12 Ma) are among the last-formed craters whose ejecta are abundant at the CE-5 site (~3% and ~2% of all ejecta).

The regolith thickness at the site is around 4–6 m (Section 3.1), while the top ~74 cm are mixed up at least one time (Qian, Xiao, Wang, et al., 2021). Thus, the surface samples collected are primarily from the ejecta of IC-259, IC-261, and minor contributions from other nearby craters younger than Xu Guangqi. With increasing depth, the abundance of particles from IC-396 increases; after ~74 cm, the regolith may be largely from Xu Guangqi. Particles from craters older than Xu Guangqi should be buried by its ejecta, including those from IC-265 and IC-266. However, the excavation of local craters postdating IC-396, may penetrate through the Xu Guangqi ejecta blanket and transport the buried particles to the site. Similarly, ejecta from four key distal craters (Harpalus, Copernicus, Aristarchus, Mairan G, Section 4.1) are also buried by the Xu Guangqi ejecta; subsequently, small craters may dig out a small portion of them. If distal materials are discovered, they are most likely from these four craters.

5. Conclusions

The morphology and morphometry of impact craters surrounding the CE-5 site were systematically studied. We created an impact crater database (Table S4 in Supporting Information S1) of 209 key ejecta source craters. We conclude that: (a) the regolith thickness at the CE-5 site is ~4–6 m; (b) CE-5 samples are dominated by local materials and materials that are different than the local basalts are mainly from Harpalus (~6%), Copernicus (~2%), Aristarchus (~1%), and Mairan G (~1%) craters; (c) impact ejecta are mainly from IC-259 (~3%), IC-261 (~2%), IC-265 (~29%), IC-266 (~4%), and Xu Guangqi (~37%), with ages possibly younger than ~200 Ma; (d) the drill samples mainly contain IC-261 and IC-265 particles at the surface and the proportion of Xu Guangqi increases with increasing depth, and may dominate the drill samples after ~74 cm.

CE-5 is the first mission to return mare samples younger than 2.8 Ga (Tartèse et al., 2019), which is dated to be ~2.0 Ga by isotopic measurements (Che et al., 2021). However, CE-5 in northern Oceanus Procellarum only represents a single point for the late-stage volcanism. There are still a multitude of questions remaining concerning the nature of late volcanism on the Moon, such as: (a) What are the heat sources responsible for the generation of the young volcanism, (b) Are the mantle sources the same for the young and the old mare basalts, (c) Do Oceanus Procellarum and Mare Imbrium have the same magma source, (d) What is the age of the youngest. More missions are required in order to improve our understanding of late lunar volcanism, especially from different sites around the Moon (Cohen et al., 2021; Draper et al., 2021).

Data Availability Statement

The LROC NAC and Kaguya TC Morning Map image IDs and download links are listed in Table S1 in Supporting Information S1. The LROC WAC images are from the LROC website (http://wms.lroc.asu.edu/lroc/view_rdr_product/WAC_GLOBAL_E300N3150_100M). ISIS3 is available from USGS Astrogeology Center and uploaded to Zenodo (http://doi.org/10.5281/zenodo.5532983). SLDEM2015 are from USGS Astropedia (https://astrogeology.usgs.gov/search/map/Moon/LRO/LOLA/Lunar_LRO_LOLAKaguya_DEMmerge_60N60S_512ppd). CraterTools and Craterstats 2.0 are from Freie Universität Berlin (https://www.geo.fu-berlin.de/en/geol/fachrichtungen/planet/software/index.html). Data produced in this study are uploaded to Zenodo (http://doi.org/10.5281/zenodo.5532994).

Acknowledgments
This research is funded by the National Key R&D Program of China (2020YFE0202100), the Pre-Research Project on Civil Aerospace Technologies (D020101, D020205), and the National Natural Science Foundation of China (41830214). Y. Qian is funded by the China Scholarship Council 201906410015. C. Wohler and T. Wilhelm are funded by the Deutsche Forschungsgemeinschaft (DFG, German Research Foundation), Project No. 269661170. C. Wohler, R. Bugiolacchi, and S. Althoff are funded by the Macau Science and Technology Development Fund (FDCT) 0079/2019/A2. J. W. Head received no outside funding for this research. Y. Qian wants to thank Feng Zhang for discussions on the crater degradation model.

References

Barker, M. K., Mazarico, E., Neumann, G. A., Zuber, M. T., Haruyama, J., & Smith, D. E. (2016). A new lunar digital elevation model from the Lunar Orbiter Laser Altimeter and SELENE Terrain Camera. *Icarus*, *273*, 346–355. https://doi.org/10.1016/j.icarus.2015.07.039

Basilevsky, A. T. (1976). On the evolution rate of small lunar craters. In *7th Lunar Science Conference* (pp. 1005–1020). Pergamon Press.

Basilevsky, A. T., Head, J. W., & Horz, F. (2013). Survival times of meter-sized boulders on the surface of the Moon. *Planetary and Space Science*, *89*, 118–126. https://doi.org/10.1016/j.pss.2013.07.011

Bugiolacchi, R., & Wöhler, C. (2020). Small craters population as a useful geological investigative tool: Apollo 17 region as a case study. *Icarus*, *350*, 113927. https://doi.org/10.1016/j.icarus.2020.113927

Che, X., Nemchin, A., Liu, D., Long, T., Wang, C., Norman, M. D., et al. (2021). Age and composition of young basalts on the Moon, measured from samples returned by Chang'e-5. *Science*, *80*, eabl7957. https://doi.org/10.1126/science.abl7957
Cohen, B. A., Young, K. E., Zellner, N. E. B., Zacny, K., Yingst, R. A., Watkins, R. N., et al. (2021). In situ geochronology for the next decade: Mission designs for the Moon, Mars, and Vesta. *Planetary Science Journal*, *2*, 145. https://doi.org/10.3847/psj/abedbf
Costello, E. S., Ghent, R. R., Hirabayashi, M., & Lucey, P. G. (2020). Impact gardening as a constraint on the age, source, and evolution of ice on mercury and the moon. *Journal of Geophysical Research: Planets*, *125*, e2019JE006172. https://doi.org/10.1029/2019JE006172
Deng, X., Zheng, Y., Jin, S., Yao, M., Zhao, Z., Li, H., et al., (2021). Design and implementation of sampling, encapsulating, and sealing system of Chang'e-5. *Space: Science & Technology*, *51*, 753–762. https://doi.org/10.1360/SST-2021-0093
Draper, D. S., Lawrence, S. J., Klima, R. S., Denevi, B. W., van der Bogert, C. H., Elardo, S. M., & Hiesinger, H. H. (2021). The inner solar system chronology (ISOCHRON) lunar sample return mission concept: Revealing two billion years of history. *Planetary Science Journal*, *2*, 79. https://doi.org/10.3847/psj/abe419
Fassett, C. I., & Thomson, B. J. (2014). Crater degradation on the lunar maria: Topographic diffusion and the rate of erosion on the Moon. *Journal of Geophysical Research: Planets*, *119*, 2255–2271. https://doi.org/10.1002/2014JE004698
Fu, X., Hou, X., Zhang, J., Li, B., Ling, Z., Jolliff, B. L., et al. (2021). Possible non-mare lithologies in the regolith at the chang'e-5 landing site: Evidence from remote sensing data. *Journal of Geophysical Research: Planets*, *126*, e2020JE006797. https://doi.org/10.1029/2020JE006797
Haruyama, J., Matsunaga, T., Ohtake, M., Morota, T., Honda, C., Yokota, Y., et al. (2008). Global lunar-surface mapping experiment using the Lunar Imager/Spectrometer on SELENE. *Earth, Planets and Space*, *60*, 243–255. https://doi.org/10.1186/BF03352788
Head, J. W., & Wilson, L. (2020). Rethinking lunar mare basalt regolith formation: New concepts of lava flow protolith and evolution of regolith thickness and internal structure. *Geophysical Research Letters*, *47*, e2020GL088334. https://doi.org/10.1029/2020GL088334
Hiesinger, H., Head, J. W., Wolf, U., Jaumann, R., & Neukum, G. (2011). Ages and stratigraphy of lunar mare basalts: A synthesis. *Special Papers—Geological Society of America*, *477*, 1–51. https://doi.org/10.1130/2011.2477(0110.1130/2011.2477(01)
Hörz, F., Basilevsky, A. T., Head, J. W., & Cintala, M. J. (2020). Erosion of lunar surface rocks by impact processes: A synthesis. *Planetary and Space Science*. *194*, 105105. https://doi.org/10.1016/j.pss.2020.105105
Huang, J., Xiao, Z., Flahaut, J., Martinot, M., Head, J., Xiao, X., et al. (2018). Geological characteristics of Von Kármán Crater, Northwestern South Pole-Aitken Basin: Chang'e-4 landing site region. *Journal of Geophysical Research: Planets*, *123*, 1684–1700. https://doi.org/10.1029/2018JE005577
Huang, Y.-H., Minton, D. A., Hirabayashi, M., Elliott, J. R., Richardson, J. E., Fassett, C. I., & Zellner, N. E. B. (2017). Heterogeneous impact transport on the Moon. *Journal of Geophysical Research: Planets*, *122*, 1158–1180. https://doi.org/10.1002/2016JE005160
HÖrz, F., Grieve, R., Heiken, G., Spudis, P., & Binder, A. (1991). Lunar surface processes. In G. H. Heiken, D. T. Vaniman, & B. M. French (Eds.), *Lunar sourcebook: A user's guide to the moon* (pp. 61–120). Cambridge University Press.
Iqbal, W., Hiesinger, H., & van der Bogert, C. H. (2020). Geological mapping and chronology of lunar landing sites: Apollo 12. *Icarus*, *352*, 113991. https://doi.org/10.1016/j.icarus.2020.113991
Joy, K. H., Crawford, I. A., Russell, S. S., & Kearsley, A. T. (2010). Lunar meteorite regolith breccias: An in situ study of impact melt composition using LA-ICP-MS with implications for the composition of the lunar crust. *Meteoritics & Planetary Science*, *45*, 917–946. https://doi.org/10.1111/j.1945-5100.2010.01067.x
Kneissl, T., van Gasselt, S., & Neukum, G. (2011). Map-projection-independent crater size-frequency determination in GIS environments—New software tool for ArcGIS. *Planetary and Space Science*, *59*, 1243–1254. https://doi.org/10.1016/j.pss.2010.03.015
Koenig, B., Neukum, G., & Fechtig, H. (1977). Recent lunar cratering: Absolute ages of Kepler, Aristarchus, TYCHO. In *Eighth Lunar and Planetary Science Conference* (pp. 555–556). Lunar Planetary Institute.
Lemelin, M., Lucey, P. G., Gaddis, L. R., Hare, T., & Ohtake, M. (2016). Global map products from the Kaguya multiband imager at 512 ppd: Minerals, FeO, and OMAT. In *47th Lunar and Planetary Science Conference*.
Liu, J., Zeng, X., Li, C., Ren, X., Yan, W., Tan, X., et al. (2020). Landing site selection and overview of China's lunar landing missions. *Space Science Reviews*, *217*, 6. https://doi.org/10.1007/s11214-020-00781-9
Liu, T., Michael, G., Wünnemann, K., Becker, H., & Oberst, J. (2020). Lunar megaregolith mixing by impacts: Spatial diffusion of basin melt and its implications for sample interpretation. *Icarus*, *339*, 113609. https://doi.org/10.1016/j.icarus.2019.113609
Liu, T., Michael, G., Zhu, M., & Wünnemann, K. (2021). Predicted sources of samples returned from Chang'e-5 landing region. *Geophysical Research Letters*, *48*, e2021GL092434. https://doi.org/10.1029/2021GL092434
Liu, T., Michael, G., Zuschneid, W., Wünnemann, K., & Oberst, J. (2021). Lunar megaregolith mixing by impacts: Evaluation of the nonmare component of mare soils. *Icarus*, *358*, 114206. https://doi.org/10.1016/j.icarus.2020.114206
McKay, D. S., Heiken, G. H., Basu, A., Blanford, G., Simon, S., Reedy, R., et al. (1991). The Lunar Regolith. In *Lunar sourcebook: A user's guide to the moon* (pp. 285–356). Cambridge University Press.
Melosh, H. J. (1989). *Impact cratering: A geologic process*. Oxford University Press.
Mercer, C. M., Young, K. E., Weirich, J. R., Hodges, K. V., Jolliff, B. L., Wartho, J.-A., & van Soest, M. C. (2015). Refining lunar impact chronology through high spatial resolution $^{40}Ar/^{39}Ar$ dating of impact melts. *Science Advances*, *1*, e1400050. https://doi.org/10.1126/sciadv.1400050
Michael, G. G., & Neukum, G. (2010). Planetary surface dating from crater size-frequency distribution measurements: Partial resurfacing events and statistical age uncertainty. *Earth and Planetary Science Letters*, *294*, 223–229. https://doi.org/10.1016/j.epsl.2009.12.041
Neukum, G., Ivanov, B. A., & Hartmann, W. K. (2001). Cratering records in the inner solar system in relation to the lunar reference system. In R. Kallenbach, J. Geiss, & W. K. Hartmann (Eds.), *Chronology and evolution of mars* (pp. 55–86). Springer. https://doi.org/10.1007/978-94-017-1035-0_3
Oberbeck, V. R. (1975). The role of ballistic erosion and sedimentation in lunar stratigraphy. *Reviews of Geophysics*, *13*, 337–362. https://doi.org/10.1029/RG013i002p00337
Oberbeck, V. R., & Quaide, W. L. (1968). Genetic implications of Lunar regolith thickness variations. *Icarus*, *9*, 446–465. https://doi.org/10.1016/0019-1035(68)90039-0
Petro, N. E., & Pieters, C. M. (2006). Modeling the provenance of the Apollo 16 regolith. *Journal of Geophysical Research: Planets*, *111*, E09005. https://doi.org/10.1029/2005JE002559
Qian, Y., Xiao, L., Head, J. W., van der Bogert, C. H., Hiesinger, H., & Wilson, L. (2021). Young lunar mare basalts in the Chang'e-5 sample return region, northern Oceanus Procellarum. *Earth and Planetary Science Letters*, *555*, 116702. https://doi.org/10.1016/j.epsl.2020.116702
Qian, Y., Xiao, L., Head, J. W., & Wilson, L. (2021). The long sinuous Rille System in Northern Oceanus Procellarum and its relation to the chang'e-5 returned samples. *Geophysical Research Letters*, *48*, e2021GL092663. https://doi.org/10.1029/2021GL092663

Qian, Y., Xiao, L., Wang, Q., Head, J. W., Yang, R., Kang, Y., et al. (2021). China's Chang'e-5 landing site: Geology, stratigraphy, and provenance of materials. *Earth and Planetary Science Letters*, *561*, 116855. https://doi.org/10.1016/j.epsl.2021.116855

Qiao, L., Chen, J., Xu, L., Wan, S., Cao, H., Li, B., & Ling, Z. (2021). Geology of the Chang'e-5 landing site: Constraints on the sources of samples returned from a young nearside mare. *Icarus*, *364*, 114480. https://doi.org/10.1016/j.icarus.2021.114480

Robinson, M. (2021). Chang'e 5 landing site topography. In *Europlanet science congress 2021*. https://doi.org/10.5194/epsc2021-863

Robinson, M. S., Brylow, S. M., Tschimmel, M., Humm, D., Lawrence, S. J., Thomas, P. C., et al. (2010). Lunar Reconnaissance Orbiter Camera (LROC) instrument overview. *Space Science Reviews*, *150*, 81–124. https://doi.org/10.1007/s11214-010-9634-2

Shen, S., Zhou, B., Li, Y., Lu, W., Liu, Q., Tang, C., et al. (2021). The design of payload lunar regolith penetrating radar on chang'e-5 lander. *IEEE Aerospace and Electronic Systems Magazine*, *36*, 4–16. https://doi.org/10.1109/MAES.2020.3033439

Sides, S. C., Becker, T. L., Becker, K. J., Edmundson, K. L., Backer, J. W., Wilson, T. J., et al. (2017). The USGS integrated software for imagers and spectrometers (ISIS 3) instrument support, new capabilities, and releases. In *48th Lunar and Planetary Science Conference*.

Tartèse, R., Anand, M., Gattacceca, J., Joy, K. H., Mortimer, J. I., Pernet-Fisher, J. F., et al. (2019). Constraining the evolutionary history of the moon and the inner solar system: A case for new returned lunar samples. *Space Science Reviews*, *215*, 54. https://doi.org/10.1007/s11214-019-0622-x

van der Bogert, C. H., & Hiesinger, H. (2020). Which samples are needed for improved calibration of the lunar cratering chronology? In *51st Lunar and Planetary Science Conference*. Lunar and Planetary Institute.

Wang, J., Zhang, Y., Di, K., Chen, M., Duan, J., Kong, J., et al. (2021). Localization of the chang'e-5 lander using radio-tracking and image-based methods. *Remote Sensing*, *13*, 590. https://doi.org/10.3390/rs13040590

Wilhelm, T., & Wöhler, C. (2021). Uncertainty guided recognition of tiny craters on the moon. In *2020 25th international conference on pattern recognition (ICPR)* (pp. 5198–5205). https://doi.org/10.1109/ICPR48806.2021.9413285

Xie, M., Xiao, Z., Zhang, X., & Xu, A. (2020). The provenance of regolith at the chang'e-5 candidate landing region. *Journal of Geophysical Research: Planets*, *125*, e2019JE006112. https://doi.org/10.1029/2019JE006112

Xie, M., Zhu, M.-H., Xiao, Z., Wu, Y., & Xu, A. (2017). Effect of topography degradation on crater size-frequency distributions: Implications for populations of small craters and age dating. *Geophysical Research Letters*, *44*, 10171–10179. https://doi.org/10.1002/2017GL075298

Yue, Z., Di, K., Liu, Z., Michael, G., Jia, M., Xin, X., et al. (2019). Lunar regolith thickness deduced from concentric craters in the CE-5 landing area. *Icarus*, *329*, 46–54. https://doi.org/10.1016/j.icarus.2019.03.032

Zanetti, M., Stadermann, A., Jolliff, B., Hiesinger, H., van der Bogert, C. H., & Plescia, J. (2017). Evidence for self-secondary cratering of Copernican-age continuous ejecta deposits on the Moon. *Icarus*, *298*, 64–77. https://doi.org/10.1016/j.icarus.2017.01.030

Zhang, F., Head, J. W., Wöhler, C., Bugiolacchi, R., Wilson, L., Basilevsky, A. T., et al. (2020). Ring-Moat Dome Structures (RMDSs) in the Lunar Maria: Statistical, compositional, and morphological characterization and assessment of theories of origin. *Journal of Geophysical Research: Planets*, *125*, e2019JE005967. https://doi.org/10.1029/2019JE005967